Transient Voltage and Current Stresses Estimation of MMC-MTDC System via Discrete-time Analysis

Yongyang Chen, *Student Member*, *IEEE*, Meng Huang, Shangzhi Pan, *Senior Member*, *IEEE*, Abdelali El Aroudi, *Senior Member*, *IEEE*, and Xiaoming Zha, *Member*, *IEEE*

***Abstract*—Transient voltage and current stresses are essential for the design and protection of multi-terminal DC (MTDC) transmission systems, particularly under the short term dynamics after severity grid faults. In this paper, we propose a discrete-time model for the modular multilevel converter based MTDC (MMC-MTDC) system considering the DC side disturbances in the system. Based on the piecewise linear modeling, the state variables such as the transient voltage on the sub-module (SM), arm current, etc., can be calculated analytically for the critical short term (within 10 ms) after the severity DC fault while the system protection is not yet activated. Parameter sensitivity analysis is also performed to give a better system design guideline. The estimation results are verified by detailed electromagnetic (EMT) circuit simulations and the scaled-down experimental laboratory prototype.**

***Index Terms*—Multi-terminal DC transmission system, modular multilevel converter, submodule voltage stress, fault current analysis, discrete-time model.**

I. INTRODUCTION

NOWADAYS, the multi-terminal DC (MTDC) transmission system is one of the most promising technologies for large-scale renewable energy integration and asynchronous grid interconnection [1-2]. The modular multilevel converter (MMC) is a preferred topology for AC-DC conversion in the MTDC system because of its modularity structure, high power capacity and high efficiency [3-4].

However, the external faults and disturbances are inevitable in the power grid. The MTDC system should therefore be designed and protected properly regarding to the unpredictable severity faults. Particularly, an accurate prediction of the transient electrical stress in the MTDC system would be helpful for the system component selection and the fault ride through control [5].

Although the system voltage and current can be acquired in the electrical magnetic transient simulations [6-8], it is more important to have an analytical model to estimate the voltage and current stresses for the system design, protection and control. In [9], on the basis of the RLC equivalent circuit, the fault clearance principle of a MMC based high voltage DC transmission system (MMC-HVDC) is presented along with a calculation of the maximum inrush current. In [10], the authors adopted an averaged approach and derived the impedance model of the MMC system to determine the current in steady-state and under short-circuit fault conditions. In [11], the equivalent circuits including inductors, capacitors, resistors and diodes are established to calculate the transient short-circuit current of a DC transmission system based on a voltage source converter (VSC). In [12], the capacitance equivalent coefficient is proposed, and the transient currents in different cases are calculated by taking different equivalent capacitance value for a MMC. In [13-14], the RLC equivalent circuit models for the MMCs are established to calculate the fault current of a DC power grid. In [15], an improved RLC equivalent circuit with controlled current source is proposed to calculate the short-circuit current of MTDC considering the system control. In order to achieve a simple model expression, these methods mentioned above are mainly developed based on the constant equivalent circuit of the system.

However, the structure of the system changes after the grid fault due to the large disturbance on the system's operation point. Specifically, this structure change will lead to a mismatch between the model prediction and practical system operation in the early few cycles after the fault occurs considering the switching features of the MMC. This mismatch could be critical since the protection and control should be designed with this fault transient.

More accurate prediction can be achieved by discrete-time modeling preserving the MMC structure. In [16-17], the discrete-time model is adopted to analyze the transient operation of MMC and the system under AC line faults. However, when a DC side fault occurs, a model is still needed for the voltage and current estimation considering the variation on the capacitor voltage of sub-modules (SMs) and interaction between AC current and DC output current of MMC.

The aim of this study is to address the above challenges. The rest of this paper is organized as follows. Section II develops the equivalent capacitor model and the model of MTDC. In section III, the transient electrical stress calculation method under DC bipolar fault is presented. The theoretical calculations from this method are validated by numerical simulation and experimental measurements in Section IV.

Manuscript received ***. (*Corresponding author: M. Huang.*)

This work was supported in part by the National Natural Science Foundation of China under Grants 51637007 and in part by the Science and Technology Projects of State Grid Corporation of China under project SG-TYHT/16-JS-198.

Y. Chen, M. Huang, S. Pan and X. Zha are with the School of Electrical Engineering and Automation, Wuhan University, Wuhan, China. (E-mail: meng.huang@whu.edu.cn).

A. El Aroudi is with the GAEI Research Center, Departament d'Enginyeria Electrònica, Universitat Rovira i Virgili, Elèctrica i Automàtica, Av. Paisos Catalans, No. 26, 43007 Tarragona, Spain.

Color versions of one or more of the figures in this paper are available online at http://ieeexplore.ieee.org.

Digital Object Identifier *******

Finally concluding remarks are provided on Section V.

II. System Modeling

Fig. 1 shows a three-terminal radial MMC-MTDC system. The AC sides of the MMCs are connected to different AC grids or loads, and the DC side is interconnected by the DC overhead lines. The DC line connection point is marked as node 4 and the DC current limiting reactor is L_r. The DC overhead lines are equivalent as series RL circuits, and the location of fault is recorded as the fault node 0, and the fault distance D_f is the distance from fault node 0 to one terminal station MMC1. Line parameters on both sides of the fault node 0 are recorded as R_{10}, L_{10}, R_{40} and L_{40}. The L_r is the DC reactor for protection purpose and can be varying according to practical design. Other system parameters are listed in Table I.

A. Modeling of MMC

The topology of MMC can be shown in Fig. 2. The voltage neutral points are denoted as O on the AC side and O' on the DC side. In general, each MMC arm consists of N half-bridge sub-modules (HBSMs), an arm inductance L_0, and an equivalent resistance R_0. The HBSM is constructed by two IGBTs and a capacitor.

For this kind of HBSM based MMC topology, the DC fault current cannot be blocked due to the fault current path provided by the diode in parallel with the IGBT when a fault occurs on the DC side. Therefore, the voltage and current stresses should be carefully modeled and calculated.

Here, the sum of the sub-module voltages in each arm is expressed as v_{pj} or v_{nj}, where subscripts 'j' denote the phase sequence of the AC side; subscripts 'p' and 'n' denote the upper and the lower arm respectively. According to the Kirchhoff's law, the equations describing the arm currents i_{pj}, i_{nj} can be expressed as follows.

$$L_0\frac{di_{pj}}{dt}=\frac{1}{2}v_{dc}-v_{gj}-v_{pj}-R_0 i_{pj}+v_{oo'} \tag{1}$$

$$L_0\frac{di_{nj}}{dt}=\frac{1}{2}v_{dc}+v_{gj}-v_{nj}-R_0 i_{nj}-v_{oo'} \tag{2}$$

Since the sum of the phase currents in the three-phase three-wire AC system is zero, and the phase current is the current difference between the upper and lower arms, we have the following constraints.

$$i_{ga}+i_{gb}+i_{gc}=0 \tag{3}$$

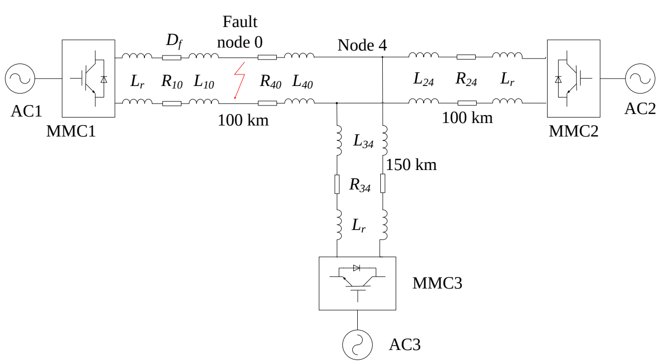

Fig. 1. Topology of a three-terminal MMC-MTDC system with possible DC line fault.

TABLE I

MMC-MTDC System parameters

Parameters	Symbols	Value
DC line voltage	V_{dc}	80 kV
AC phase voltage peak value	V_{g1}	40 kV
MMC1 active power	P_{L1}	1.6 MW
Number of arm SMs	N	20
Resistance per kilometer	R_{oh}	0.006 Ω
Inductance per kilometer	L_{oh}	0.945 mH
SM capacitance	C_{sm}	9 mF
MMC sampling frequency	f_s	5 kHz
Arm total resistance	R_0	0.5 Ω
Arm total inductance	L_0	5 mH

$$i_{gj}=i_{nj}-i_{pj} \tag{4}$$

According to (3) and (4), the neutral point voltage $v_{oo'}$ can be derived by subtracting (1) from (2), is shown as

$$v_{oo'}=\sum_{j=a,b,c}\frac{v_{pj}-v_{nj}}{6} \tag{5}$$

In (1) and (2), the arm currents i_{pj}, i_{nj} are the state variables, and the grid voltage v_{gj} is the input variable. In order to solve the state equations, the expressions of the arm voltage v_{pj}, v_{nj} are also needed.

The inserting or bypassing state of SM can be expressed in terms of the switching functions $S_{j,ri}$, where the subscript 'r' denotes the upper or the lower arm, and the subscript 'i' denotes the number of SM. If a SM is inserted, the switching function of this SM is equal to 1. Otherwise, the switching function for this SM is zero. The, the number of inserted SMs in a MMC arm is expressed as

$$n_{pj}(t)=\sum_{i=1}^{N}S_{j,pi}(t) \tag{6}$$

$$n_{nj}(t)=\sum_{i=1}^{N}S_{j,ni}(t) \tag{7}$$

Due to the nonlinearity of the switching function, it is difficult to derived the voltage expression for each capacitor in SMs. Here, we use the concept of equivalent capacitor based of

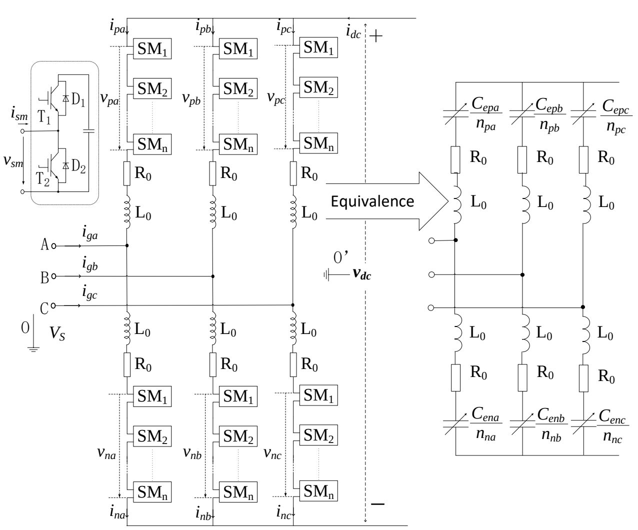

Fig. 2. Topology of a three-phase MMC. The DC side capacitors can be equivalent as varying capacitors.

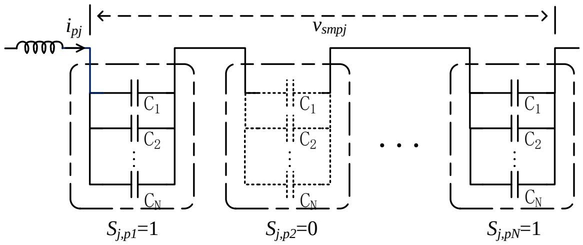

Fig. 3. Equivalent capacitor circuit.

[12] to represent the charging and discharging process of the DC capacitors in MMC structure and the capacitance of the equivalent capacitor is described.

B. Modeling of Capacitor in SMs

The total arm voltage is the sum of voltages on the inserted SM capacitors. Assuming that the SM capacitors is sharing the total DC voltage, the arm voltage can be expressed as

$$v_{pj} = n_{pj}\left(t\right)\cdot v_{smpj} \tag{8}$$

$$v_{nj} = n_{nj}\left(t\right)\cdot v_{smnj} \tag{9}$$

where v_{smpj} denotes the upper arm SM capacitor voltage of j-phase, and v_{smnj} denotes the lower arm SM capacitor voltage of j-phase.

According to the definition of equivalent capacitor, the SM voltage charging and discharging process can be expressed as

$$C_{epj}\frac{dv_{smpj}}{dt} = i_{pj} \tag{10}$$

$$C_{enj}\frac{dv_{smnj}}{dt} = i_{nj} \tag{11}$$

where C_{epj} stands for the upper arm equivalent capacitor of j-phase and C_{enj} is the lower arm equivalent capacitor of the same phase.

Since the voltage balancing algorithm is adopted in MMC, it is equivalent to connecting the N SM capacitors of the same arm in parallel. Thus, the SM equivalent capacitor after reaching voltage balance is increased by N times. However, the value of the equivalent capacitance is not only affected by the voltage balancing algorithm, but also by the nearest level modulation (NLM) algorithm according to which the sum of the inserted SMs is always N for one phase, but the number of inserted SMs in each arm varies with the AC output voltage. Therefore, the value of the equivalent capacitance of each arm is also changing. Therefore, the equivalent capacitor circuit can be represented by Fig. 3 and the equivalent capacitor of one arm is

$$C_{epj} = \frac{NC_{sm}}{n_{pj}\left(t\right)} \tag{12}$$

$$C_{enj} = \frac{NC_{sm}}{n_{nj}\left(t\right)} \tag{13}$$

Similar with the equivalent capacitor method described in [8], the proposed SMs capacitor equivalence here also satisfies the energy conservation principle.

$$\frac{1}{2}n_{pj}\left(\mathrm{t}\right)C_{epj}v_{sm}^2 = \frac{N}{2}C_{sm}v_{sm}^2 \tag{14}$$

By adopting this equivalent capacitor concept, the arm voltage can be expressed as the capacitor voltage associated with the switching function. Although the state-space model of MMC has been obtained, it is expressed by the switching function making it difficult to be solved analytically. In order to find the analytical solution of the state equations, the switching function of the NLM algorithm also must be discretized.

C. Piecewise Analysis

In order to make the time-varying capacitor circuit solvable, the piecewise analysis method is applied to time-varying capacitors according to the characteristics of NLM. Here, a three-phase five-level MMC (3p-5L-MMC) is adopted as a derivation example, in which 24 operation states should be considered in the calculation. A higher level piecewise analysis method can be performed in the same way.

According to the modulation principle, if the number of inserted SMs changes, the MMC switches to a next stage and the switching function increases or decreases by 1.

For the ease of calculation, we use δ_{jm} to replace the upper and the lower arm switch function in (6) and (7).

$$\delta_{jm} = n_{pj}\left(t_{jm}\right) \tag{15}$$

$$N-\delta_{jm} = n_{nj}\left(t_{jm}\right) \tag{16}$$

When the modulation ratio is 1, the voltage angle during the m-th stage can be expressed as follows.

$$\theta_{am} = \frac{\arccos\left[\left(\frac{N}{2}-\delta_{am}-\frac{1}{2}\right)\frac{2}{N}\right]}{\pi} \tag{17}$$

The duty cycle corresponding to each stage of a MMC can be calculated as the same method mentioned in [17]. For three-phase MMC, the modulation reference voltages of phase B is delayed by $2\pi/3$ with respect to phase A, while that of phase C is delayed by $4\pi/3$. Thus, the corresponding different stages and changing instants of three-phase five-level MMC can be easily found. The stage switching times of the three phases are ordered and are respectively denoted as θ_1, θ_2... θ_m. Thus, the duty ratio of the m-th step is

$$d_m = \theta_m - \theta_{m-1} \tag{18}$$

It is worth noticing that the voltage and current stresses would be very critical for the system during the short term (within 10 ms) after the severe fault occurs, since the system protection would not be activated immediately. Also, the power/voltage control may not be able to adjust in such a short time scale. Therefore, the modulation duty cycles can be simply developed according to the regular NLM. In longer time scale, the control of MMC could be considered. However, in this paper, only the critical short time estimation will be discussed.

III. Transient Voltage and Current Estimation

Assuming that the line capacitance can be ignored, the load on the DC side of MMC is a series circuit of resistance and inductance. The sum of DC inductance is denoted as L_d and the sum of DC resistance as R_d. The expression of the DC side voltage v_{dc} is

$$v_{dc} = -\sum_{j=a,b,c} i_{pj}R_d - L_d\frac{d\sum_{j=a,b,c} i_{pj}}{dt} \tag{19}$$

Substituting (5) and (19) into (1) and (2), and combining with (10) and (11), the state equation of the MMC-MTDC system can be obtained as

$$\dot{x}(t) = Ax(t) + Bu(t) \tag{20}$$

where $x(t)= [i_{pa}, i_{na}, i_{pb}, i_{nb}, i_{pc}, i_{nc}, v_{smpa}, v_{smna}, v_{smpb}, v_{smnb}, v_{smpc}, v_{smnc}]^T$ is the vector of state variables and $u(t)=[v_{ga}, v_{gb}, v_{gc}]^T$ is the vector of external input parameters.

Applying the piecewise analysis, each stage of the state matrix A can be expressed as

$$A_m = \begin{bmatrix} F & U_m \\ L_m & O \end{bmatrix} \tag{21}$$

where O is a 6×6 null matrix. The expressions of the other matrices appearing in (21) are given in (26) to (28). The matrix B can be expressed as (29).

The time-varying capacitor system is decomposed into m LTI systems in the piecewise analysis and can be solved by varies analytical methods. In this paper, we introduces a commonly used analytical algorithm for discrete-time systems [17], [18]. For the LTI system, the time-domain solution of (20) can be expressed as follows

$$x(t) = \phi_m(t-t_0)\,x(t_0) + \psi_m(t-t_0)\,B \tag{22}$$

where t_0 is an appropriate initial time, and $x(t_0)$ denotes the initial condition of $x(t)$ at time instant t_0.

During the MMC working process, the coefficients of matrix A are different at different switching stages of each line period. But the solution can be obtained with the initial state defined in the previous stage. Here, with respect to each stage of a line period, the matrix A is varying but takes the sequence of A_1, A_2 ... to A_{24}, for this 3p-5L-MMC. The corresponding matrices $\phi_m(t)$ and $\psi_m(t)$ then are as follows.

$$\phi_m(t) = e^{A_m t} \tag{23}$$

$$\psi_m(t) = \int_0^t \phi_m(t-\tau)u(\tau)\,d\tau \tag{24}$$

We denote $x(t_n)$ as the initial state value within the n-th period. The final value of each stage can be derived as

$$\begin{cases} x(t_n + d_1T_s) = \phi_1(d_1T_s)\,x(t_n) + \psi_1(d_1T_s)\,B \\ x(t_n + d_1T_s + d_2T_s) = \phi_2(d_2T_s)\,x(t_n + d_1T_s) + \psi_2(d_2T_s)\,B \\ \cdots \\ x(t_n + \sum_{r=1}^{m} d_rT_s) = \phi_m(d_mT_s)\,x\left(t_n + \sum_{r=1}^{m-1} d_1T_s\right) + \psi_m(d_mT_s)\,B \end{cases} \tag{25}$$

$$F = \begin{bmatrix}
-\frac{2L_0R_0+2L_dR_0+L_0R_d}{L_0(2L_0+3L_d)} & 0 & -\frac{L_0R_d-L_dR_0}{L_0(2L_0+3L_d)} & 0 & -\frac{L_0R_d-L_dR_0}{L_0(2L_0+3L_d)} & 0 \\
0 & -\frac{2L_0R_0+2L_dR_0+L_0R_d}{L_0(2L_0+3L_d)} & 0 & -\frac{L_0R_d-L_dR_0}{L_0(2L_0+3L_d)} & 0 & -\frac{L_0R_d-L_dR_0}{L_0(2L_0+3L_d)} \\
-\frac{L_0R_d-L_dR_0}{L_0(2L_0+3L_d)} & 0 & -\frac{2L_0R_0+2L_dR_0+L_0R_d}{L_0(2L_0+3L_d)} & 0 & -\frac{L_0R_d-L_dR_0}{L_0(2L_0+3L_d)} & 0 \\
0 & -\frac{L_0R_d-L_dR_0}{L_0(2L_0+3L_d)} & 0 & -\frac{2L_0R_0+2L_dR_0+L_0R_d}{L_0(2L_0+3L_d)} & 0 & -\frac{L_0R_d-L_dR_0}{L_0(2L_0+3L_d)} \\
-\frac{L_0R_d-L_dR_0}{L_0(2L_0+3L_d)} & 0 & -\frac{L_0R_d-L_dR_0}{L_0(2L_0+3L_d)} & 0 & -\frac{2L_0R_0+2L_dR_0+L_0R_d}{L_0(2L_0+3L_d)} & 0 \\
0 & -\frac{L_0R_d-L_dR_0}{L_0(2L_0+3L_d)} & 0 & -\frac{L_0R_d-L_dR_0}{L_0(2L_0+3L_d)} & 0 & -\frac{2L_0R_0+2L_dR_0+L_0R_d}{L_0(2L_0+3L_d)}
\end{bmatrix} \tag{26}$$

$$U_m = \begin{bmatrix}
\frac{-(6L_d+5L_0)\delta_{am}}{L_0(6L_0+9L_d)} & -\frac{N-\delta_{am}}{(6L_0+9L_d)} & \frac{(3L_d+L_0)\delta_{bm}}{L_0(6L_0+9L_d)} & -\frac{(N-\delta_{bm})}{(6L_0+9L_d)} & \frac{(3L_d+L_0)\delta_{cm}}{L_0(6L_0+9L_d)} & -\frac{(N-\delta_{cm})}{(6L_0+9L_d)} \\
-\frac{\delta_{am}}{(6L_0+9L_d)} & \frac{-(6L_d+5L_0)(N-\delta_{am})}{L_0(6L_0+9L_d)} & -\frac{\delta_{bm}}{(6L_0+9L_d)} & \frac{(3L_d+L_0)(N-\delta_{bm})}{L_0(6L_0+9L_d)} & -\frac{\delta_{cm}}{(6L_0+9L_d)} & \frac{(3L_d+L_0)(N-\delta_{cm})}{L_0(6L_0+9L_d)} \\
\frac{(3L_d+L_0)\delta_{am}}{L_0(6L_0+9L_d)} & -\frac{(N-\delta_{am})}{(6L_0+9L_d)} & \frac{-(6L_d+5L_0)\delta_{bm}}{L_0(6L_0+9L_d)} & -\frac{(N-\delta_{bm})}{(6L_0+9L_d)} & \frac{(3L_d+L_0)\delta_{cm}}{L_0(6L_0+9L_d)} & -\frac{(N-\delta_{cm})}{(6L_0+9L_d)} \\
-\frac{\delta_{am}}{(6L_0+9L_d)} & \frac{(3L_d+L_0)(N-\delta_{am})}{L_0(6L_0+9L_d)} & -\frac{\delta_{bm}}{(6L_0+9L_d)} & \frac{-(6L_d+5L_0)(N-\delta_{bm})}{L_0(6L_0+9L_d)} & -\frac{\delta_{cm}}{(6L_0+9L_d)} & \frac{(3L_d+L_0)(N-\delta_{cm})}{L_0(6L_0+9L_d)} \\
\frac{(3L_d+L_0)\delta_{am}}{L_0(6L_0+9L_d)} & -\frac{(N-\delta_{am})}{(6L_0+9L_d)} & \frac{(3L_d+L_0)\delta_{bm}}{L_0(6L_0+9L_d)} & -\frac{(N-\delta_{bm})}{(6L_0+9L_d)} & \frac{-(6L_d+5L_0)\delta_{cm}}{L_0(6L_0+9L_d)} & -\frac{(N-\delta_{cm})}{(6L_0+9L_d)} \\
-\frac{\delta_{am}}{(6L_0+9L_d)} & \frac{(3L_d+L_0)(N-\delta_{am})}{L_0(6L_0+9L_d)} & -\frac{\delta_{bm}}{(6L_0+9L_d)} & \frac{(3L_d+L_0)(N-\delta_{bm})}{L_0(6L_0+9L_d)} & -\frac{\delta_{cm}}{(6L_0+9L_d)} & \frac{-(6L_d+5L_0)(N-\delta_{cm})}{L_0(6L_0+9L_d)}
\end{bmatrix} \tag{27}$$

$$L_m = diag\left(\frac{\delta_{am}}{NC_{sm}}, \frac{N-\delta_{am}}{NC_{sm}}, \frac{\delta_{bm}}{NC_{sm}}, \frac{N-\delta_{bm}}{NC_{sm}}, \frac{\delta_{cm}}{NC_{sm}}, \frac{N-\delta_{cm}}{NC_{sm}}\right) \tag{28}$$

$$B = \begin{bmatrix}
-\frac{1}{L_0} & \frac{1}{L_0} & 0 & 0 & 0 & 0 & 0 & 0 & 0 & 0 & 0 & 0 \\
0 & 0 & -\frac{1}{L_0} & \frac{1}{L_0} & 0 & 0 & 0 & 0 & 0 & 0 & 0 & 0 \\
0 & 0 & 0 & 0 & -\frac{1}{L_0} & \frac{1}{L_0} & 0 & 0 & 0 & 0 & 0 & 0
\end{bmatrix}^T \tag{29}$$

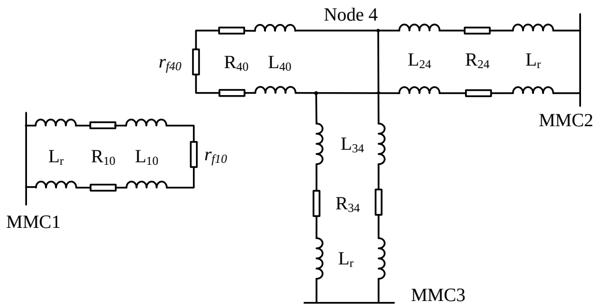

Fig. 4. Simplified equivalent circuit of DC network for fault current calculation with fault resistance.

In the above expression, $x(t_n + \sum_{r=1}^{m} d_r T_s)$ represents the vector of state variables at the end of the m-th stage during the n-th period which is also the initial value of the (n+1)-th time period of the MMC modulation. Therefore, the state variables including the voltage and current can be calculated according to (25) without solving the differential equations.

Based on the above discrete-time modeling, the transient voltage and current stresses estimation process can be briefly listed as follows.

1) When a DC fault occurs, the DC line topology is reformed. According to the method in [14], the DC network can be simplified as shown in Fig. 4 after the fault. The corresponding resistance of r_{f10} and r_{f40} can be written as

$$r_{f10} = \left(1 + \frac{L_r + L_{10}}{L_r + L_{40} + L_{24}} + \frac{L_r + L_{10}}{L_r + L_{40} + L_{34}}\right) R_{f0} \tag{30}$$

$$r_{f40} = \left(1 + \frac{2L_d + 2L_{40} + L_{34} + L_{24}}{L_d + L_{10}}\right) R_{f0} \tag{31}$$

where R_{f0} is the fault resistance. The disturbance occurring time t_n is also recorded.

2) After the fault occurs, the output of NLM is still regular in a sinusoidal way. The duty ratio of each stage can be denoted as d'_m according to (17) and (18).

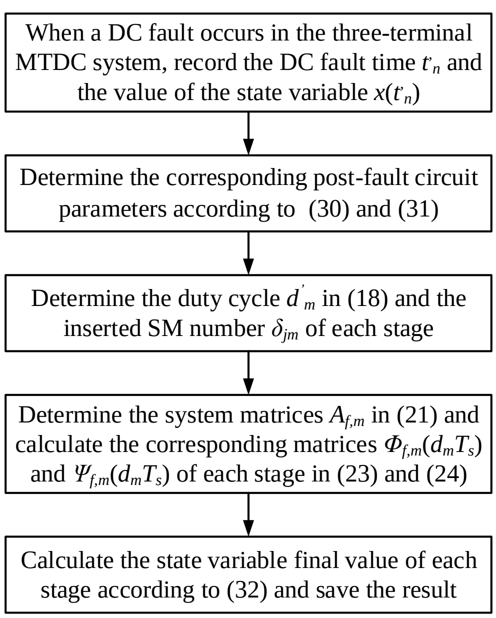

Fig. 5. The flow chart of post-fault voltage and current stresses calculation.

3) The matrices A of each stage after a DC disturbance can be calculated as $A_{f,1}$, $A_{f,2}$,... $A_{f,m}$ according to the equation (21) and (26)-(28) with respect to the switching state of each SMs. The corresponding state transition matrices $\phi_{f,m}(t)$ and discrete-time input matrices $\psi_{f,m}(t)$ are calculated as (23)-(24) and indicated as $\phi_{f,1}$, $\phi_{f,2}$,... $\phi_{f,m}$ and $\psi_{f,1}$, $\psi_{f,2}$,... $\psi_{f,m}$.

4) The value of the state variable at the time of the short circuit $x(t'_n)$ is adopted as the initial value for the stress estimation. The final values in every stage, after the DC disturbance, can be expressed as

$$x_f(t'_n + \sum_{r=1}^{m} d'_r T_s) = \phi_{f,m}(d'_m T_s)\, x_f\left(t'_n + \sum_{r=1}^{m-1} d'_r T_s\right) + \psi_{f,m}(d'_m T_s) B \tag{32}$$

where $x_f(t'_n + \sum_{r=1}^{m} d'_r T_s)$ represents the vector of state variables which can be voltage or current state of the system.

After the state transition matrix and input matrix of each stage are determined, the state variables can be obtained by matrix algebraic operations instead of solving the differential equation.

In a summary, using the derived discrete-time expression of the MMC-MTDC, the value of state variables can be accurately calculated after a DC disturbance. These state variables include not only the system AC and DC current of MMC-MTDC, but also the sub-module voltage and the arm current in the converter which cannot be described by the RLC equivalent model. The steps are briefly summarized in Fig. 5.

IV. SIMULATION AND EXPERIMENT VERIFICATION

In order to verify the above analysis and calculation method, detailed electromagnetic (EMT) simulations in MATLAB Simulink software and experiment of a MMC prototype are performed. The system topology and parameters in the simulation is the same as that depicted in Fig. 1 and Table I.

A. DC side Transient Voltage and Current Stresses

As shown in Fig. 1, when a DC fault occurs at fault node 0, the DC side transient current and voltage stresses can be calculated and verified. In Fig. 6, the protecting DC reactor L_r is 5 mH and the fault distance is 5 km from the MMC1 station. The fault time is recorded as time 0 on the x-axis. The results of the traditional RLC equivalent circuit method are indicated by dashed curves. The theoretical calculation results are indicated by the dots. The EMT simulation results are represented by solid lines showing a remarkable agreement with the estimated analytical results.

Fig. 6 (a) shows the DC side current. The values from the RLC equivalent method are slight larger than the ones from the EMT simulation results at the beginning of the fault and then smaller than the ones from EMT simulation results. This is because the RLC equivalent method takes a large capacitance value and does not consider the influence of the AC system feed current. The current obtained during the discharge stage of the capacitor is large, and there is no source of energy during the AC system feed stage.

Fig. 6 (b) shows the DC side voltage for different value of R_{f0}.

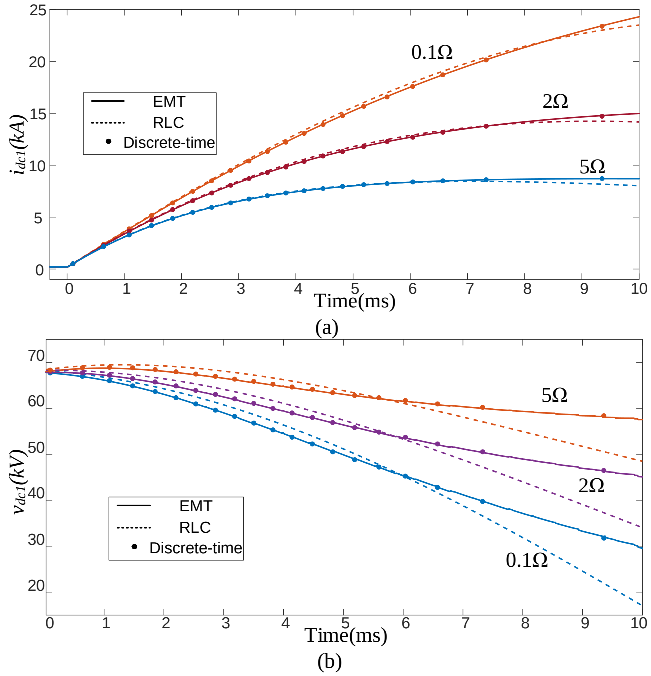

Fig. 6. Comparison of the estimation results and electromagnetic simulation within 10 ms after DC fault. (a) DC side current i_{dc}; (b) DC side voltage v_{dc}.

In this figure, the maximum error of DC current calculated by the RLC equivalent method is about 1 kA, and the maximum error of DC voltage exceeds 10 kV within the critical postfault time of 10 ms. However, the proposed discrete-time method still maintains high precision. The reason is that, in the proposed model, the capacitor discharging is performed noticing the sub-module switching due to the modulation. Meanwhile, by considering the modulation, the power transfer of the AC side of the MMC station is also taken into account. Therefore, the over-simplification in the RLC model is avoided.

When the fault resistance is set as constant (R_{f0}=0.1 Ω), the relationship between the DC current value at 10 ms after the DC fault with various DC reactor values and the fault distance is shown in Fig. 7. It can be seen that the DC current would increase significantly when the DC reactor is getting smaller and the fault is geographically close to the MMC station.

B. AC side Transient Voltage and Current Stresses

When a DC fault occurs, the AC side of the system will also be influenced, especially the current on each arm of the converter and voltage on the SMs. These stresses would be critical since they affect the power device design and protection directly. However, the RLC model would fail to estimate it since the detailed structure is ignored.

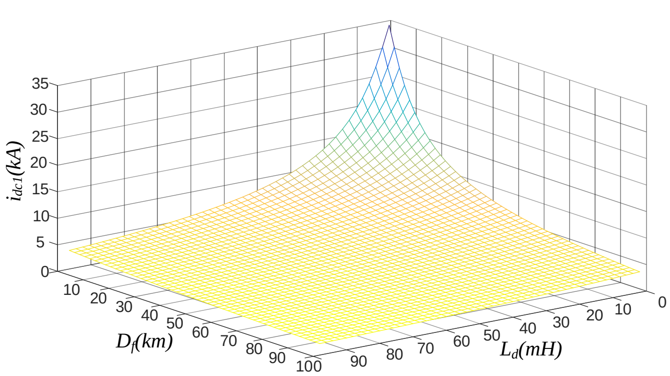

Fig. 7. DC current value (10 ms after fault) with DC reactor and fault distance change.

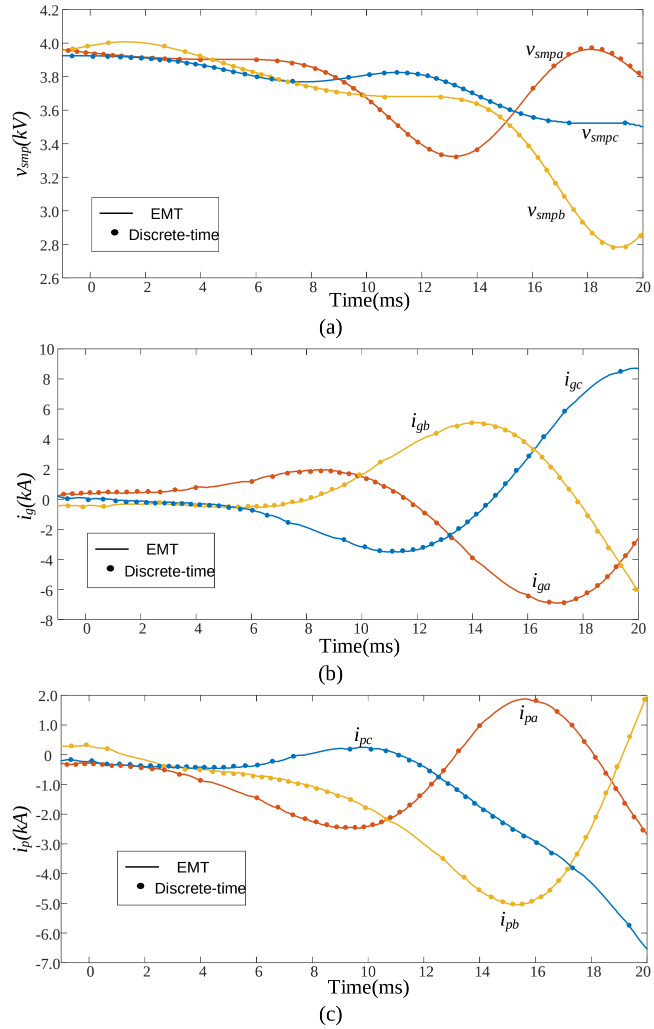

Fig. 8. Comparison of the estimation results and electromagnetic simulation within 20 ms after a DC fault occurs. (a) upper arm SM capacitor voltage v_{smp}; (b) AC side current i_g; (c) upper arm current i_p.

In Fig. 8, we compare the simulation and discrete-time model calculation results. The fault point is 50 km away from MMC1 station. The DC reactor inductance is 50 mH and its resistance is 0.1 Ω.

Fig. 8 shows the results of AC current, upper arm SM capacitor voltage and upper arm current with the calculation results in the dots and the EMT simulation results in the solid lines.

In Fig. 8 (a), the SM capacitor voltage drops after the discharging process starts during the DC fault. The calculation results estimated by the discrete-time model are consistent with

TABLE II

PEAK VALUE OF PHASE CURRENTS AFTER FAULT

t_{fault}/s	i_{ga}/kA	i_{gb}/kA	i_{gc}/kA	i_{pa}/kA	i_{pb}/kA	i_{pc}/kA
0.300	1.958	5.100	-3.502	-2.471	-5.052	0.250
0.304	-4.747	3.189	-1.689	0.733	-3.506	-6.107
0.310	-1.958	-5.099	3.501	-6.364	0.897	-3.760

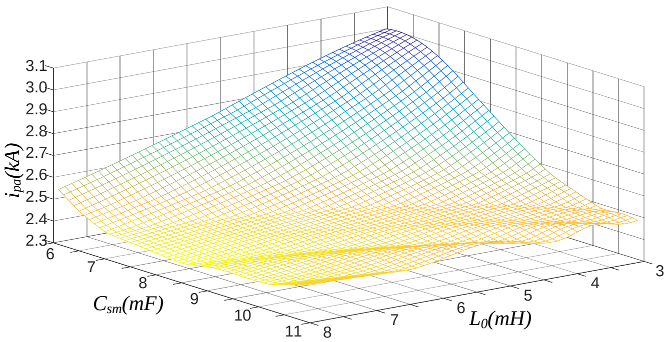

Fig. 9. Peak value of phase A upper arm current after fault (within 10 ms) with arm total inductance and SM capacitance change.

the detailed circuit simulations.

Fig. 8 (b) and (c) shows the calculated current on the AC line and the upper arm. The above voltage and current stresses would be varying due to the modulation on the SMs. Therefore, the stresses should be calculated for each arm of the converter, and also for different fault time. In Fig. 8, the three phase results are shown. And for different fault time, the peak values of currents are listed in Table II. Apparently, the worst case should be considered in the design.

The system parameters also influence the voltage and current stresses. Fig. 9 shows the calculation results of arm current on the phase-A under different SM capacitance and total arm inductance. It is shown that the peak value of the fault current can be reduced with larger arm total inductance and SM capacitance. From the analytically calculated results, the voltage and current stresses in the system can be evaluated in the initial design, which can be helpful for choosing the system parameters.

C. Computation Load

The state transition matrices $\phi_m(t)$ and $\psi_m(t)$ are related to the system parameters and the duty ratio of each stage. After the fault occurs, the state transition matrices of the corresponding stage are pre-solved, and the state transition matrices and the initial value of the corresponding stage are multiplied according to (25). For each stage, the solution of the state variables only needs to perform matrix multiplication once to get the initial value of the next stage.

For one specific fault, the system structure and parameters can be predicted by the system designer or operator. Therefore, the state transition matrices $\phi_m(t)$ and $\psi_m(t)$ of different periods can be derived based on the system discrete-time model. As for different periods, the only difference in parameter calculation is the initial value of the state variable. The computational complexity only increases linearly with the number of levels.

The simulation platform used in this paper is equipped with the 2.60 GHz Intel(R) core CPU, 4GB RAM and 64-bit with Windows 8 operating system. The EMT simulation time step is 10 μs and the total duration is 0.5 s. The calculation time of the EMT simulation, the RLC equivalent method and the discrete-time method are listed in Table III. When the number of SMs increases, the EMT simulation time increases significantly, while the discrete-time method calculation time increases with the system voltage levels. For the 21 levels system, the computation burden is reduced by two orders comparing to the EMT simulation, with acceptable calculation accuracy.

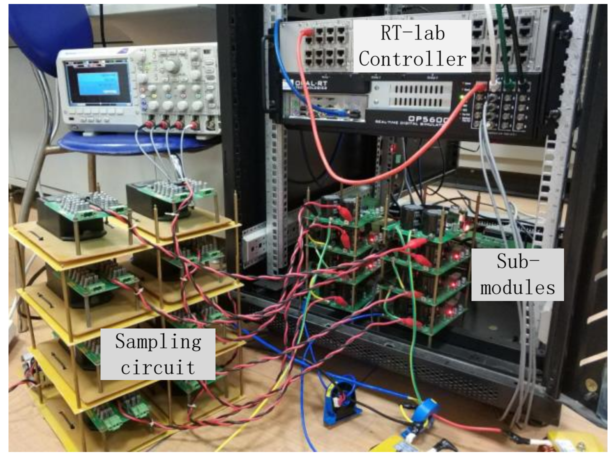

Fig. 10. The prototype of single-phase MMC

D. Scale-Down Experiment

Under the laboratory conditions, we built a single-phase five-level MMC prototype and simulated the fault condition with a smaller load resistor on the DC side. The parameters of the MMC prototype are listed in Table IV. The hardware prototype is shown in Fig. 10 and the MMC prototype controller is RT-lab. The fault time in the experiment takes place at the zero crossing of the AC current and the fault resistance R_f is set as 6.7 Ω. Due to the NLM algorithm of the single-phase five-level MMC, the calculation process of one cycle is divided into eight stages. The discrete-time model of the single-phase five-level MMC and the duty cycle of each stage are described in detail in [19].

Fig. 11 depicts the discrete-time calculation results and the experiment results. The calculated results of each stage are also listed in Table V. Comparing Fig. 11 and Table V, the calculation and experiment results of the DC current peak are 4.45A and 4.5A, respectively. The calculation and experiment results of the upper bridge arm current peak are -8.28A and -7.5A, respectively. The error between experiment and calculation is within 10%. It can be observed that the proposed

TABLE III

CALCULATION LOAD COMPARISON

Method	EMT simulation	Equivalent RLC method	Discrete-time method
Time(5-level)	14.93s	0.529s	0.785s
Time(9-level)	53.39s	0.536s	1.872s
Time(21-level)	643.04s	0.686s	4.293s

TABLE IV

EXPERIMENT PARAMETERS OF SINGLE-PHASE MMC

Symbols	Value	Symbols	Value
V_{dc}/V	30	L_0/mH	4
f_s/Hz	50	R_0/Ω	0.3
Z_L/Ω	15	V_g/V	17
N	4	C_{sm}/mF	3

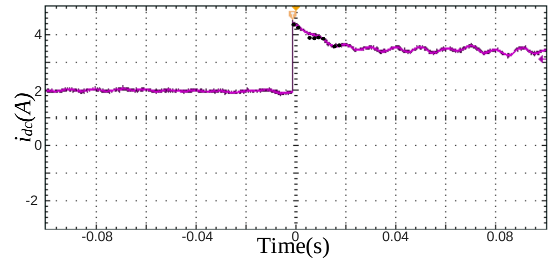

(a)

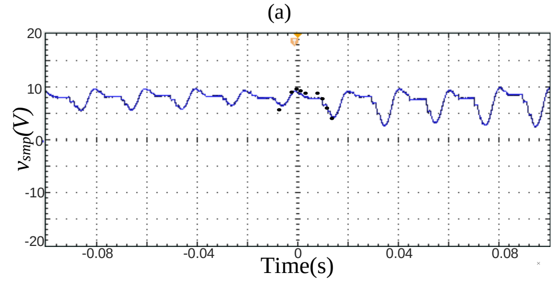

(b)

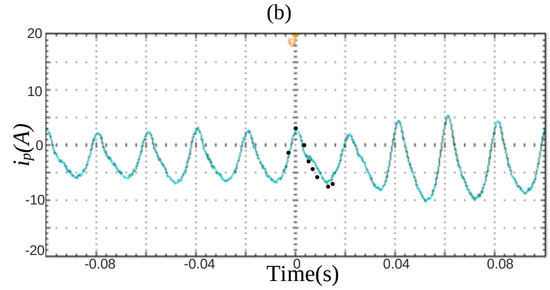

(c)

Fig. 11. Calculation and experiment results of single-phase MMC. (a) DC current i_{dc} (A); (b) Upper arm SM capacitor voltage v_{smp} (V); (c) Upper arm current i_p (A).

TABLE V

CALCULATED RESULTS OF EACH STAGE AFTER FAULT

m	1	2	3	4	5	6	7	8
i_{dc}(A)	4.45	3.99	3.90	3.91	3.96	3.63	3.59	3.66
v_{smp}(V)	5.07	9.20	10.0	9.59	8.98	8.98	7.70	5.48
i_p(A)	-2.09	3.06	-0.53	-3.08	-5.15	-7.07	-8.28	-7.43

discrete-time method can reflect the variation of the transient voltage and current in the experiment prototype with the preset circuit parameters.

V. CONCLUSION

In this paper, a novel discrete-time-based transient voltage and current stress estimation method is proposed for predicting the transient SM capacitor voltage, arm current and line current under DC bipolar faults in MTDC system. By using an equivalent capacitor, the proposed model can reflect the dynamics of internal state variables such as the SM capacitor voltage and the arm current. Detailed comparisons show that the proposed discrete-time method is more accurate than the traditional RLC model, and much lower computation burden. The method is also robustness to parameter changes. The proposed method and related parameter sensitivity analysis can be used for MTDC parameter design and protection.

REFERENCES

[1] M. K. Bucher, R. Wiget, G. Andersson and C. M. Franck, “Multiterminal HVDC networks-what is the preferred topology?” *IEEE Trans. Power Del.*, vol. 29, no. 1, pp. 406-413, Feb. 2014.

[2] T. M. L. Assis, S. Kuenzel, and B. C. Pal, “Impact of multi-terminal HVDC grids on enhancing dynamic power transfer capability,” *IEEE Trans. Power Syst.*, vol. 32, no. 4, pp. 2652–2662, Jul. 2017.

[3] M. A. Perez, S. Bernet, J. Rodriguez, S. Kouro and R. Lizana, “Circuit topologies, modeling, control schemes, and applications of modular multilevel converters,” *IEEE Trans. Power Electron.*, vol. 30, no. 1, pp.4-17, Jan. 2015.

[4] A. Nami, J. Liang, F. Dijkhuizen and G. D. Demetriades, “Modular multilevel converters for HVDC applications: review on converter cells and functionalities,” *IEEE Trans. Power Electron.*, vol. 30, no. 1, pp. 18-36, Jan. 2015.

[5] T. H. Nguyen, K. A. Hosani, M. S. E. Moursi and F. Blaabjerg, “An overview of modular multilevel converters in HVDC transmission systems with STATCOM operation during pole-to-pole DC short circuits,” *IEEE Trans. on Power Electron.*, vol. 34, no. 5, pp. 4137-4160, May 2019.

[6] Z. Zhang and Z. Xu, “Short-circuit current calculation and performance requirement of HVDC breakers for MMC-MTDC systems,” *IEEJ Trans. Elect. Electron. Eng.*, vol. 11, no. 2, pp. 168–177, Mar. 2016.

[7] S. Liu, Z. Xu, W. Hua, G. Tang and Y. Xue, “Electromechanical Transient Modeling of Modular Multilevel Converter Based Multi-Terminal HVDC Systems,” *IEEE Trans. Power Syst.*, vol. 29, no. 1, pp. 72-83, Jan. 2014.

[8] J. Peralta, H. Saad, S. Dennetiere, J. Mahseredjian and S. Nguefeu, “Detailed and averaged models for a 401-level MMC–HVDC system,” *IEEE Trans. on Power Del.*, vol. 27, no. 3, pp. 1501-1508, July 2012.

[9] Y. Xue and Z. Xu, “On the bipolar MMC-HVDC topology suitable for bulk power overhead line transmission: configuration, control, and DC fault analysis,” *IEEE Trans. Power Del.*, vol. 29, pp. 2420-2429, 2014.

[10] A. Wasserrab and G. Balzer, “Determination of dc short-circuit currents of MMC-HVDC converters for DC circuit breaker dimensioning,” in *Proc. IET Int. Conf. AC DC Power Transmiss*., 2015, pp. 1–7.

[11] J. Yang, J. E. Fletcher and J. O'Reilly, “Short-circuit and ground fault analyses and location in VSC-based DC network cables,” *IEEE Trans. Ind. Electron.*, vol. 59, no. 10, pp. 3827-3837, Oct. 2012.

[12] G. Duan, Y. Wang, T. Yin, S. Yin, G. Li and S. Sun, “DC short circuit current calculation for modular multilevel converter,” *Power Syst. Tech.*, vol. 42, no. 7, pp. 2145-2152, 2018. (in Chinese)

[13] C. Li, C. Zhao, J. Xu, Y. Ji, F. Zhang and T. An, “A pole-to-pole short-circuit fault current calculation method for DC grids,” *IEEE Trans. Power Syst.*, vol. 32, no. 6, Nov. 2017.

[14] Y. Li, J. Li, L. Xiong, X. Zhang and Z. Xu, “DC fault detection in meshed mtdc systems based on transient average value of current,” *IEEE Trans. Ind. Electron.*, pp.1-11, 10.1109/TIE.2019.2907499. Early access. 2019.

[15] M. Langwasser, G. De Carne, M. Liserre and M. Biskoping, “Fault current estimation in multi-terminal HVdc grids considering MMC control,” *IEEE Trans. Power Syst.*, vol. 34, no. 3, pp. 2179-2189, May 2019.

[16] A. Zama, A. Benchaib, S. Bacha, D. Frey and S. Silvant, “High dynamics control for MMC based on exact discrete-time model with experimental validation,” *IEEE Trans. Power Del*., vol. 33, no. 1, pp. 477-488, Feb. 2018.

[17] Y. Liu, M. Huang, X. Zha and H. H. C. Iu, “Short-circuit current estimation of modular multilevel converter using discrete-time modeling,” *IEEE Trans. Power Electron.*, vol. 34, no. 1, pp. 40-45, Jan. 2019.

[18] X. Li, X. Ruan, Q. Jin, M. Sha and C. K. Tse, "Approximate discrete-time modeling of dc–dc converters with consideration of the effects of pulse width modulation," *IEEE Trans. Power Electron.*, vol. 33, no. 8, pp. 7071-7082, Aug. 2018.

[19] Y. Chen, M. Huang and X. Zha, "Modular multilevel converter dc bipolar short-circuit current calculation on discrete-time model,” in *Proc. Electron. App. Conf. Expo.*, 2018, pp. 1-5.